Full Lumped Element-Based Equivalent Circuit Model for Connected Slot Antenna Arrays

MD RASHEDUZZAMAN AL-AMIN[1] (Graduate Student Member, IEEE), **CHAO LI**[2] (Member, IEEE),
AND MOHAMMAD S. SHARAWI[1] (Senior Member, IEEE)

[1]Department of Electrical Engineering, Poly-Grames Research Center, Polytechnique Montréal, Montreal, QC H3T 1J4, Canada

[2]School of Information Science and Engineering, Shandong Normal University, Jinan 250358, China

CORRESPONDING AUTHOR: M. R. AL-AMIN (e-mail: md-rasheduzzaman.al-amin@polymtl.ca)

ABSTRACT A full lumped element-based equivalent circuit model for connected slot antenna arrays (CSAA) is proposed with three configurations of the CSAA being considered: infinite, semi-infinite, and finite slots. First, an equivalent circuit model was developed from the available Green's Function (GF) based analytical expression of the active impedance of CSAA. It was demonstrated that by combining PI or T networks with parallel RLC resonant circuits and modeling the higher order modes via the series inductor, the active impedance and the reflection characteristics of the CSAA can be represented in an efficient and accurate manner. Secondly, utilizing the proposed equivalent circuit model, a generalized design procedure was developed to assist the design and analysis of arbitrary configurations of CSAA at both microwave and millimeter wave (mm-wave) bands. Finally, the effectiveness and accuracy of the proposed approach are validated by several numerical and measured results. A 2x2 CSAA prototype was fabricated at 3 *GHz* to validate the proposed equivalent circuit model. For the finite slot case, the proposed RLC+T network outperforms both the available transmission line-based equivalent circuit model and the proposed RLC+PI network, in describing the resonance frequencies and the values of the impedances of the finite slot. It was demonstrated that the proposed equivalent circuit model had a maximum of 4.55% and 5.27% average errors for the real and imaginary parts of the impedances, as compared with the full-wave simulator, while the computational time was reduced by more than two orders of magnitude.

INDEX TERMS Active impedance, connected slot antenna array, equivalent circuit.

I. INTRODUCTION

SLOT antennas are very versatile, have numerous applications, and have been employed both as individual elements and in array scenarios. Connected antenna arrays (CAA) are those arrays in which the elements are electrically connected. CAA offers a wide bandwidth, wide scanning angle, and lower cross-polarization levels [1], [2]. Such connected elements maintain a nearly constant current distribution within a wide frequency band. CAA can be formed with dipoles or slots. The mutual coupling between the elements enhances the bandwidth and enables better cross-polarization behavior [1], [2]. Analytical spectral domain Green's function (GF) based expressions have been derived for analyzing the characteristics of the CAA assuming infinite apertures with periodic excitation. The analytical expressions of the CAA were derived for both the free-space case and the case where a back reflector (BR) was considered beneath the CAA [2], [3]. Equivalent networks of infinite and periodic CAA were constructed for the transmission and reception modes based on the GF utilizing transmission line models in [4], [5].

Several works presented equivalent circuit models for resonant slots. In the equivalent transmission line model of the center-fed slot, the feed was described with a shunt generator, slot arms were modeled by two transmission lines, and the end terminations were represented by a short circuit [6], [7], [8]. The reactances associated with the end terminations were not considered in these equivalent models [6], [7], [8]. However, the work [9] modeled the shorted end terminations with inductances to represent the input

impedance of the slot antenna more accurately. The equivalent circuits, presented in [2], [4] and [5], considered the end terminations and described the presence of edge-born waves in finite connected arrays for both the transmission and reception modes. In addition, the equivalent circuit model of the CAA from [5] quantified the current present in the loads and the scattered fields from the structure. Equivalent transmission lines [5] were used to describe the fundamental wave propagation, and analysis regarding the existence of the unattenuated and attenuated edge waves was presented.

Using the GF solution for infinite connected slots [2], the method of moments (MoM) was used to analyze the slot antenna. In this analysis, the current in the feeding gap and the current in the end terminations were considered. Basis functions of the MoM solution included the reactance of the feed and the diffraction of the waves from the end terminations [10]. A transmission line-based equivalent circuit model was developed for infinite slots, semi-infinite, and finite slots [10], [11], [12]. These equivalent circuit models of slot antennas were modeled with transmission lines having various characteristic impedances, and impedance transformers. The end terminations of the slot antennas were represented by an RL load [10], [11], [12]. However, these equivalent circuit models based on transmission lines did not consider the presence of BR beneath the CSAA. It is worth noting that, in practical applications, CSAA needs a BR to obtain directional radiation patterns and improve its gain.

In this paper, a full, lumped-element-based equivalent circuit model is proposed for various configurations of the CSAA. Compared with the transmission line model that exists in literature, the lumped-element-based equivalent circuit model can predict the resonance information, impedance, and reflection characteristics accurately and effectively. This model will reduce the simulation and development time and make it possible to gain more insights about its behavior. This will also assist in reducing the initial steps (i.e., reduce the number of iterations) when developing the full wave model. Another important contribution of the present work is the consideration of the BR in the proposed equivalent circuit model for infinite, semi-infinite, and finite slot configurations. The equivalent circuit model is developed with the help of the spectral domain GF solution of the CAA reported in [2], which considers the presence of the BR beneath the CSAA. The parallel RLC resonant circuit, being the foundation of the developed circuit, can easily predict the resonance of the structure. The mutual coupling present between the array elements is accounted for and modeled by the T and PI networks. Consequently, with the help of the T and PI networks, an in-depth understanding regarding the inter-element coupling effects can be gained. The higher order modes of the CSAA are modeled with the help of a series inductor [2], [17], [18] to obtain an accurate estimation of the input impedance. The lumped-element-based equivalent circuit model shows an accuracy of at least 95% for all the real and imaginary impedances for the infinite periodic CSAA around the resonant frequency

(within $\pm 25\%$ of resonant frequency) compared with the full-wave simulator. The simulation time is reduced by at least two orders of magnitude for the infinite, semi-infinite and finite slot (printed on a dielectric substrate) when compared with results obtained through full-wave simulations. For the finite slot printed on a dielectric substrate with a BR, the full-wave simulator is 600 times slower in calculating the input impedance than the proposed equivalent circuit model.

The remainder of the paper is organized as follows: after demonstrating the viability of the proposed equivalent circuit model for the infinite CSAA in Section II, semi-finite and finite slots are considered in Sections III and IV, respectively. The impedance and reflection characteristics of different configurations are compared with the full-wave simulations and available results. The effect of various slot parameters (like the width of the slot, length of the slot, etc.) on the different circuit element values of the proposed circuit model is analyzed in Section V. A 2x2 prototype was fabricated and measured; its results are compared with both the proposed circuit model's and full-wave simulation's results in Section VI, showing an overall acceptable agreement. A general design procedure for any arbitrary configurations of CSAA at both microwave and mm-wave frequencies is described in Section VII. And finally, Section VIII concludes the paper.

II. INFINITE SLOT

The active impedance of the infinitely long and periodic CSAA is reported in [2]. A typical diagram of the CSAA is shown in Fig. 1. It is illustrated that the long slots are oriented periodically in both x and y directions (parallel to one another representing a planar array). There is a BR at a distance of h_s beneath the slots where the air is the separating medium. The active impedance for the infinite and periodic CSAA is expressed as [2], [13]:

$$Z_{slot}^{br} = \frac{k_0 \zeta_0 d_y}{d_x} \sum_{m_x=\infty}^{\infty} sinc^2(k_{xm}\delta_s/2)$$
$$\times \frac{1}{(k_o^2 - k_{xm}^2)\sum_{m_y=-\infty}^{\infty} \dfrac{J_o\left(k_{ym}\dfrac{w_s}{2}\right)(1 - jcot(k_{zm}h_s))}{k_{zm}}} \tag{1}$$

where w_s is the width of the slot, δ_s is the width of the source, h_s is the height of the BR, d_x is the inter-element spacing in the x direction, d_y is the inter-element spacing in the y direction, k_0 is the free space propagation constant, ζ_0 is the intrinsic impedance in free space, $k_{xm} = k_0 sin\theta_0 cos\phi_0$, $k_{ym} = k_0 sin\theta_0 sin\phi_0$, J_0 is the Bessel function of zeroth order of the first kind, $k_{zm} = (k_o^2 - k_x m^2 - k_y m^2)^{1/2}$ and m_x and m_y represent the number of modes present in the CSAA along x and y directions, respectively. It is considered that the radiation from the arrays is directed towards the direction denoted by $\theta = \theta_0$ and $\phi = \phi_0$. It is assumed that the width of the slot w_s, the width of the source δ_s, etc., are small with respect to the wavelength [2], [13]. These approximations
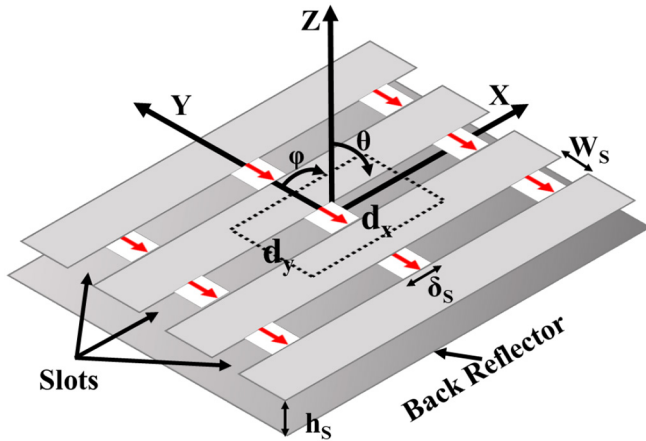
FIGURE 1. Infinite and periodic CSAA with back reflector. The separating medium between them is air. A unit cell is denoted with a dashed line showing the feeding port.

make the Bessel and Sinc functions in (1) go to unity. The consideration of the dominant mode ($m_x = m_y = 0$) and approximation of the quantities like the width of the slot and width of the source, allow (1) to have the following reduced expression [2], [13]:

$$Z_{slot}^{br} = \frac{\zeta_0 d_y}{d_x} \frac{cos\theta}{(1 - sin^2\theta cos^2\phi)(1 - jcot(k_0 h_s cos\theta))} \quad (2)$$

As shown by (2), the active impedance of the infinite CSAA is frequency-dependent through the term k_0, and in the low-frequency regime, the bandwidth is limited by the BR. The presence of the BR beneath the CSAA acts as a short circuit and thus reduces its bandwidth [2], [3], [13].

A. FUNDAMENTAL MODE: EXPANSION OF THE COTANGENT SERIES

Initially, it was considered that the radiation is directed towards the broadside direction ($\theta = 0, \phi = 0$) and it had a square periodic orientation ($d_y = d_x$). These considerations reduce (2) to have the following expression:

$$Z_{slot}^{br} = \frac{\zeta_0}{(1 - jcot(k_0 h_s))} \quad (3)$$

The cotangent series in the denominator of (3) is expanded according to [14]. This expansion gives us the following expression:

$$cot(k_0 h_s) = cot(kh) = \frac{1}{kh} - \frac{kh}{3} - \frac{(kh)^3}{45} - \frac{2(kh)^5}{945} - \frac{(kh)^7}{4725} \cdots \quad (4)$$

where $k = \frac{\omega}{v}$; v is the speed of light and ω is the operating frequency. Neglecting the higher order terms of the cotangent series and substituting (4) into (3), we arrive at

$$Z_{slot}^{br} = \frac{\zeta_0}{1 + j\left(\frac{\omega h}{3v} + \frac{(\omega h)^3}{45v^3} + \frac{(2(\omega h)^5)}{945v^5} + \frac{(\omega h)^7}{4725v^7} + \cdots - \frac{v}{\omega h}\right)} \quad (5)$$

It is well known that the input impedance of a parallel RLC resonator [15] can be represented as

$$Z_{slot}^{br} = \frac{R}{1 + j\left(\omega RC - \frac{R}{\omega L}\right)} \quad (6)$$

Comparing (5) and (6), the values of R, L, and C of the parallel RLC resonator can be obtained as follows:

$$R = \zeta_0 \quad (7a)$$

$$L = \frac{Rh}{v} \quad (7b)$$

$$C = \frac{h}{3Rv} + \frac{\omega^2 h^3}{45Rv^3} + \frac{2\omega^4 h^5}{945Rv^5} + \frac{\omega^6 h^7}{4725Rv^7} \quad (7c)$$

Now, the values of the elements of the parallel resonant circuit R, L, and C are obtained from (7a)-(7c). The values are used to calculate the active impedance of the CSAA after choosing an operating frequency (i.e., 28 GHz for 5G applications, for example). To check the accuracy of the derived input impedance expression and its dependence on the number of the terms of the cotangent series (4), we compared it with the analytical closed-form expression given in [2, eq. (3.1)], [13]. The impedance of the CSAA calculated considering the first five terms of the cotangent series is plotted in Fig. 2. The plot shows that the impedance curve does not overlap well over the entire frequency band. Rather good agreement is obtained until the resonant frequency. After the resonant frequency, the deviation is obvious. The potential reasons for the deviation could be the omission of the higher order terms of the cotangent series and ignoring the mutual coupling effects within the CSAA. To check the case of omission of terms from the cotangent series, the impedance of the CSAA was plotted again considering higher order terms in Fig. 2. The results show that the accuracy is not improved by simply adding more terms. Specifically, the consideration of the higher order terms (like the first 7th, 9th term, etc.) does not provide an observable improvement in the impedance behavior as shown in Fig. 2. The reflection coefficient of the CSAA is calculated from the obtained circuit element values using the proposed equivalent circuit approach. The reflection coefficient for different cases is plotted in Fig. 3, which also shows disagreement with the analytical one beyond resonance. Thus, it is evident that a single parallel RLC resonant circuit is not capable of representing the impedance and reflection characteristics of the CSAA.

B. REPRESENTATION OF MUTUAL COUPLING EFFECT BY PT AND T NETWORKS

To overcome the limitations of a single RLC model and obtain the full impedance and reflection characteristics of the CSAA, PI and T networks are added along with the single parallel RLC resonant circuit. These networks represent the missing component in the analysis of the CSAA. As the elements are mutually coupled in the CSAA, the resulting mutual impedances are not represented by
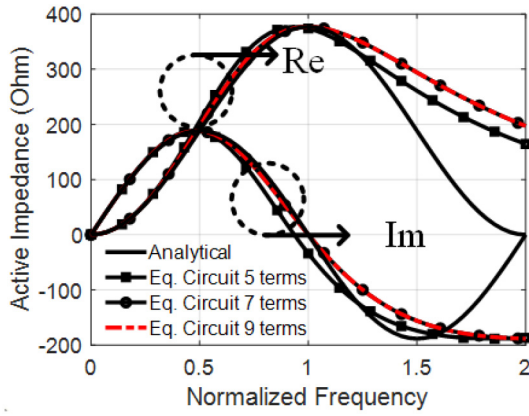
FIGURE 2. Active impedance of the CSAA calculated using the analytical expression [2, eq. (3.1)] and the proposed equivalent circuit (abbreviated as Eq. Circuit) by considering the first five, seven, and nine terms of the cotangent series. Re represents the real part and Im represents the imaginary part of the impedance, respectively.
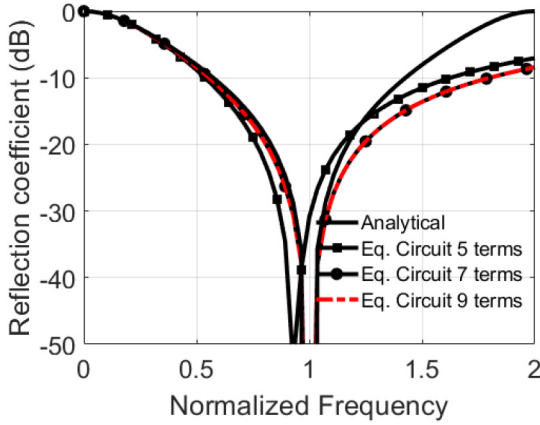

FIGURE 3. Reflection coefficient of the CSAA calculated using the analytical expression [2, eq. (3.1)] and the proposed equivalent circuit (abbreviated as Eq. Circuit) by considering the first five, seven, and nine terms of the cotangent series.

a single RLC resonant circuit alone. The addition of PI and T networks with the RLC circuit can represent the mutual coupling condition. It can be seen in Fig. 2 that the active impedance of the proposed equivalent circuit does not match well with the analytical one in the higher frequency regime. These PI and T networks work like frequency selective networks and filter out the undesired portions from the curve to resemble the analytical one by capturing the impedance at the higher frequency range. This behavior is analyzed mathematically in the following sections.

1) EQUIVALENT CIRCUIT MODEL WITH AN RLC CIRCUIT AND PI NETWORK

In this section, the analysis of the parallel RLC circuit and a PI network is presented. The circuit diagram of the RLC+PI network is shown in Fig. 4. The analytical expression of the input impedance of the RLC+PI network is derived as shown
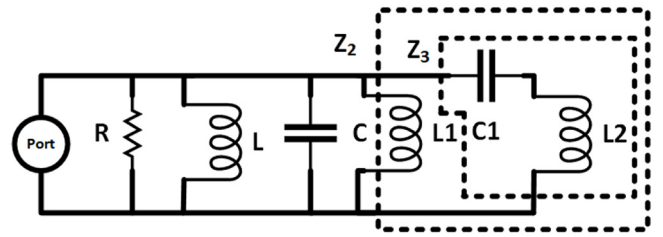

FIGURE 4. Parallel RLC resonant circuit and PI network topology.

in (8).

$$Z_3 = j\omega L_2 + \frac{1}{j\omega C_1} = \frac{1 + j^2 \omega^2 C_1 L_2}{j\omega C_1} \tag{8a}$$

$$\frac{1}{Z_2} = \frac{1}{j\omega L_1} + \frac{1}{Z_3} = \frac{1 - \omega^2 C_1 L_2 - \omega^2 C_1 L_1}{j\omega L_1 - j\omega^3 C_1 L_2 L_1} \tag{8b}$$

$$Z = \frac{R}{1 + jR\left(\omega C - \frac{1}{\omega L} - \frac{\left(1 - \omega^2 C_1 L_2 - \omega^2 C_1 L_1\right)}{\left(\omega L_1 - \omega^3 C_1 L_2 L_1\right)}\right)} \tag{8c}$$

2) EQUIVALENT CIRCUIT MODEL WITH AN RLC CIRCUIT AND T NETWORK

The analysis of the parallel RLC circuit with a T network is presented following the schematic diagram depicted in Fig. 5. The analytical expression of the input impedance of the RLC+ T network is derived in (9).

$$Z_3 = \frac{j\omega L_2}{1 + j^2 \omega^2 C_1 L_2} \tag{9a}$$

$$Z_2 = \frac{j\omega L_1 + j\omega L_2 - j\omega^3 L_1 C_1 L_2}{1 - \omega^2 C_1 L_2} \tag{9b}$$

$$Z = \frac{R}{1 + jR\left(\omega C - \frac{1}{\omega L} - \frac{\left(1 - \omega^2 C_1 L_2\right)}{\omega L_1 + \omega L_2 - \omega^3 L_1 C_1 L_2}\right)} \tag{9c}$$

3) COMPARISON BETWEEN THE RLC+PI AND RLC+T CIRCUIT MODELS

In the previous subsections, two topologies were presented. To analyze the performance of these topologies, the values of all the equivalent circuit elements are calculated first. The center frequency is set to 28 GHz (again, this is an arbitrary center frequency, resembling the current interest in 5G bands. Any other center frequency can be chosen. See fabricated prototype for example). It is considered that there is a BR at a quarter wavelength distance beneath the infinite slot to have a directional radiation pattern [2]. The value of the resistance of the CSAA is equal to the intrinsic impedance of free space as discussed in [2]. With this in mind, the values of L and C of the parallel RLC circuit are calculated using (7) and found to be $L = 3.35nH$ and $C = 9.57fF$. The values of the elements of the PI and T networks are calculated using (10a)-(10d) [16], which are widely used for
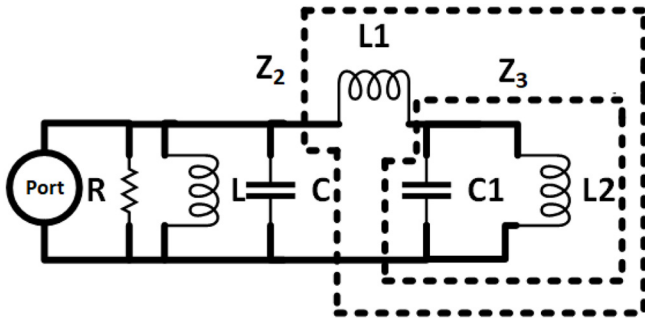
FIGURE 5. Parallel RLC resonant circuit and T network topology.

calculating the inductance and capacitance of the PI and T networks:

$$L_\pi = \frac{R_0}{2\omega_C} \tag{10a}$$

$$C_\pi = \frac{1}{2R_0\omega_C} \tag{10b}$$

$$L_T = \frac{2R_0}{\omega_C} \tag{10c}$$

$$C_T = \frac{2}{R_0\omega_C} \tag{10d}$$

The impedance and reflection coefficients of the CSAA are calculated for the following cases: analytical, RLC, RLC+PI, and RLC+T topologies. The values of the elements of the RLC+PI and RLC+T networks are tuned to obtain the desired impedance and reflection coefficient. The impedance and reflection coefficient results of these cases are plotted in Fig. 6 and Fig. 7, respectively. The graphs show good agreement with the analytical results. From Figs. 6 and 7, it is depicted that the RLC+PI and RLC+T network topologies clearly represent the impedance and reflection characteristics of the CSAA more accurately than a single RLC resonator. These two topologies consider the mutual coupling between the elements through the mutual impedances present in their expressions. These mutual impedances are present in the denominator of the analytical expressions in (8c) and (9c). These mutual impedances have nontrivial effects on the impedance and reflection parameters. It is demonstrated in Fig. 7 that the single RLC circuit shows wider bandwidth than the analytically (GF based) obtained bandwidth and it cannot capture the CSAA characteristics completely over the full frequency band. On the contrary, the RLC+PI and RLC+T networks provide a better resemblance to the analytical one in terms of active impedance and reflection coefficient. These PI and T network topologies are not unique. The proposed model is one among other possible meta-models. However, these network topologies have the properties of shaping/filtering the impedance curves of the CSAA at the higher frequency region. Any X-type network might be used to provide a similar type of effect given that it has two properties: 1) it introduces the mutual coupling present between the elements of CAA through mutual impedances and 2) it helps in capturing the impedance curve behavior at higher frequency bands. The values of different
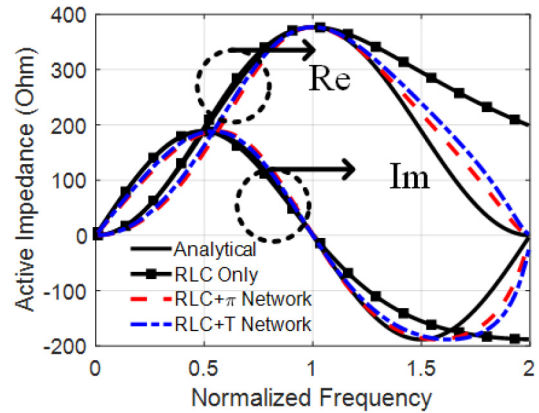

FIGURE 6. The active impedance of the CSAA calculated using analytical expression [2, eq. (3.1)], RLC circuit only, RLC+PI and RLC+T network topologies.
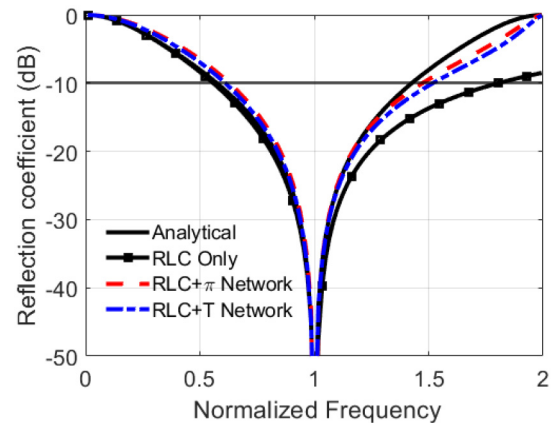

FIGURE 7. The reflection coefficient of the CSAA calculated using analytical expression [2, eq. (3.1)], RLC circuit only, RLC+PI and RLC+T network topologies.

inductive and capacitive elements used for the PI and T networks are tabulated in Table 1.

The percentage of error between the analytical and equivalent circuit (RLC+PI and RLC+T networks) models is quantified in terms of impedance. The relative error is calculated using (11):

$$Error = \frac{Z_{analytical} - Z_{network}}{Z(@resonance)} \times 100\% \tag{11}$$

where $Z_{analytical}$ is the impedance of the analytical expression and $Z_{network}$ is the impedance obtained from the RLC+PI and RLC+T networks. The percentage of error between the analytical and the proposed lumped-element-based equivalent circuit model is plotted in Fig. 8. It is demonstrated that the percentage of error is within an acceptable range for most of the values of the frequency. Excellent agreement between them is observed near the resonant frequency. The percentage of error around the resonant frequency (within ±25% of the resonant frequency) is less than 4.8% for all the impedances. However, the differences between them increase towards the trailing edge of the curves. The maximum percentage of error is 20.8%, which occurs at 1.71 times the

TABLE 1. Values of tuned and untuned L and C elements of the PI and T networks. The unit of inductance is (*nH*) and the unit of capacitance is (*fF*).

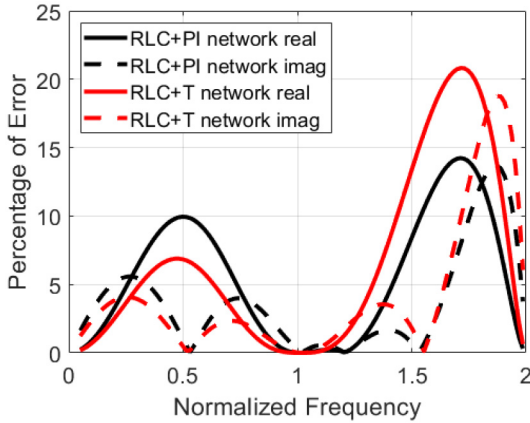| Parameters	Values		Parameters	Values	
	Untuned	Tuned		Untuned	Tuned
L_{T1}	2.14	4.4	$L\pi_1$	2.14	13.06
C_{T1}	30.15	2.4	$C\pi_1$	7.53	1.88
L_{T2}	2.14	13.87	$L\pi_2$	2.14	4.28

FIGURE 8. Quantification of error between the analytical [2, eq. (3.1)] and the proposed equivalent circuit approach.

FIGURE 9. Active impedance of the CSAA calculated using tuned and untuned lumped elements of the proposed equivalent circuit.

resonant frequency. The average error for the real and imaginary parts of the impedances from the RLC+PI network is 5.54% and 3.65%, respectively. On the other hand, the average error for the real and imaginary parts of the impedances from the RLC+T network is 6.55% and 4.03%, respectively.

4) TUNING EFFECT OF PI AND T NETWORK ELEMENTS ON THE PROPOSED CIRCUIT MODEL

In this subsection, discussions are presented about tuning the elements of PI and T networks on the proposed equivalent circuit model. It was mentioned in Section II-B.3, that the impedance and reflection coefficients of the proposed equivalent circuit model were obtained by tuning the values. Now, it is to be understood what degree/type of tuning is required to obtain the desired results and how the proposed equivalent circuit model assists in reaching the desired results. So, the active impedance of the RLC+PI network, which was plotted in Fig. 6 obtained using tuned values of the circuit elements, is plotted again in Fig. 9. In parallel, the active impedance of the RLC+PI network is calculated using the untuned values and plotted in the same figure. It is evident from the figure that the untuned values capture the resonance correctly but has a mismatch in terms of bandwidth. This mismatch can easily be overcome through a few tuning attempts. The untuned and tuned values of the elements of both the networks are calculated using (10a)-(10d) and tabulated in Table 1. This table gives us an idea about the degree/type of the required tuning. So, the discussions on the tuning effect of PI and T network elements reflect that the proposed model has mathematical formulas ((10a)-(10d)) to calculate the values of the PI and T network elements.
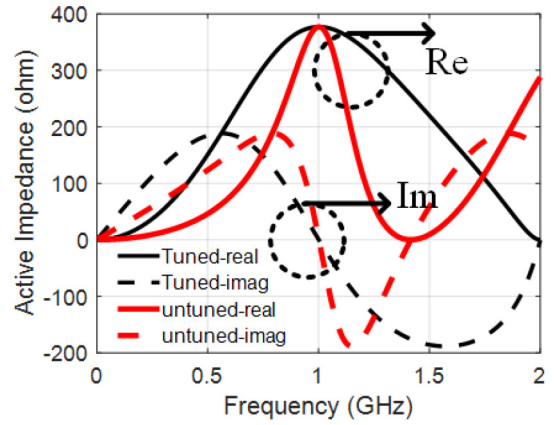
In addition, the proposed model will assist in obtaining the impedance and reflection behaviors of the CSAA with good accuracy through a few tuning attempts.

C. HIGHER ORDER MODES: ACTIVE IMPEDANCE OF THE INFINITE AND PERIODIC CSAA

In the previous subsections, the fundamental mode was modeled by a parallel RLC circuit, and the mutual coupling between the elements of the CSAA was modeled using PI or T networks. In this section, the higher-order modes are modeled as a series inductor for obtaining an accurate estimation of the input impedance. The idea of using a series inductor to represent higher order modes follows previous works [2], [17], [18]. So, a fully lumped component-based equivalent circuit model of the CSAA is presented in Fig. 10, which represents the fundamental mode (via parallel RLC circuit), the mutual coupling between the elements (via PI and T networks), and the higher order modes (as a single series inductor).

To validate the results of the proposed full lumped element-based equivalent circuit, the unit cell of the infinite and periodic CSAA is considered as shown in Fig. 1. The active impedance of the unit cell of CSAA operating at 28 GHz is calculated in CST. Following geometrical parameters $d_x = d_y = 0.5\lambda_0$, $w_s = 0.1\lambda_0$, $h_s = 0.25\lambda_0$ is considered similar to [2]. Appropriate boundary conditions and excitation of the unit cell (CSAA) are used in CST for obtaining the active impedance of the unit cell. CST results are compared with the analytical and HFSS results reported in [2] and are depicted in Fig. 11. The results in the figure show good agreement. Then, the active impedance is calculated employing the proposed lumped element-based equivalent RLC+PI and RLC+T networks. The calculated active impedance is compared with the analytical, CST, and HFSS results in Fig. 11. The comparison shows that the higher order modes representation via a series inductor has improved the active impedance of the equivalent RLC+T and RLC+PI networks. The percentage of error between the CST results and the proposed lumped element-based RLC+PI and
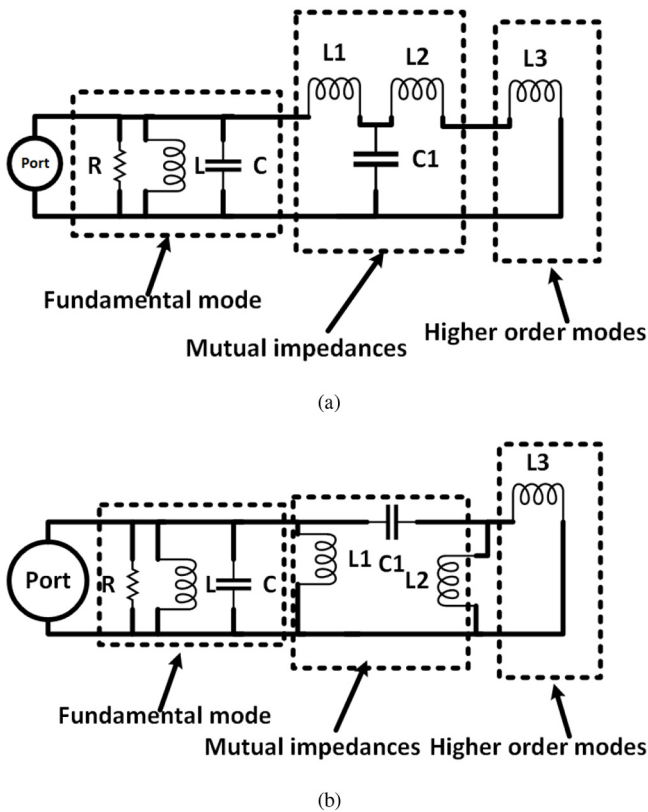
(a)

(b)

FIGURE 10. Complete lumped element-based equivalent circuit model of the CSAA: (a) equivalent RLC+T networks and (b) equivalent RLC+PI network.
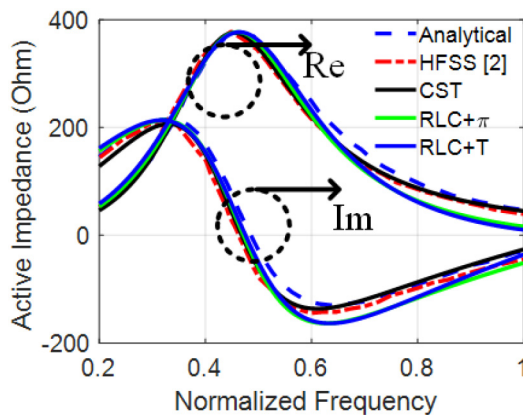

FIGURE 11. Active impedance of the infinite and periodic CSAA following analytical expression [2, eq. (2.39)], HFSS [2], CST, RLC+PI and RLC+T networks.

RLC+T circuits' results is calculated using (11) and plotted in Fig. 12. It is shown that excellent agreement between them is obtained near the resonant frequency. The percentage of error around the resonant frequency is less than 5.3% for all the impedances. However, the differences between them increase towards the trailing edge of the curves, where the maximum percentage of error is 9.2%. The average error for the real and imaginary parts of the impedances of the RLC+PI network is 3.35% and 5.27%, respectively. On the other hand, the average error for the real and imaginary
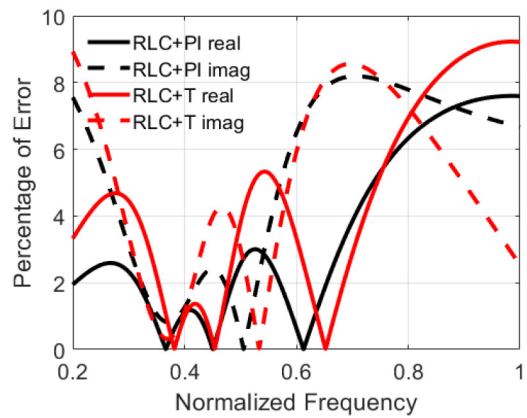

FIGURE 12. Quantification of error between the CST results and the equivalent circuit approach.

parts of the impedances of the RLC+T network is 4.55% and 4.91%, respectively. It is understood from Fig. 8 and Fig. 12 that the inclusion of the higher order mode representation via a series inductor has improved the representation of the active impedance of the CSAA and has reduced the maximum error occurring over the entire frequency range.

III. SEMI-INFINITE SLOT

In this section, the applicability of the equivalent circuit model for the semi-infinite slot antenna is presented. In [10], an MoM-based numerical solution was developed to find the input impedance of planar slots. With the aid of the numerical solution, an equivalent circuit based on transmission lines was derived to find the input impedance of a semi-infinite slot and a finite slot. The semi-infinite slot was modeled with the introduction of a short circuit having length L_{SHORT} as shown in Fig. 13. The short circuit was implemented at a distance d so that the magnetic current induced in that region did not influence the magnetic current in region 1. It was demonstrated in [10] that an RL load could be used to represent the endpoint termination of semi-infinite slot antennas. The endpoint termination was described as the RL impedance comprising inductive reactance and another non-zero resistance, which is accountable for explaining the radiation coming out from the endpoint of the slot antenna [10].

To the best of the authors' knowledge, there are no results or references available for the semi-infinite connected slot to compare with. The work in [10] presents an MoM-based solution for modeling the semi-infinite slot considering two basis functions: one for representing the contribution coming from the source point and another for the contribution coming from the endpoint. So, the provided solution for a semi-infinite slot considered a single source only. The input impedance of slots having multiple sources was not provided. It was explained that a similar procedure could be followed to derive the input impedance for planar slots having multiple feeds [10]. For this reason, the available results of the semi-infinite and finite slots from [10], [11], [12] are
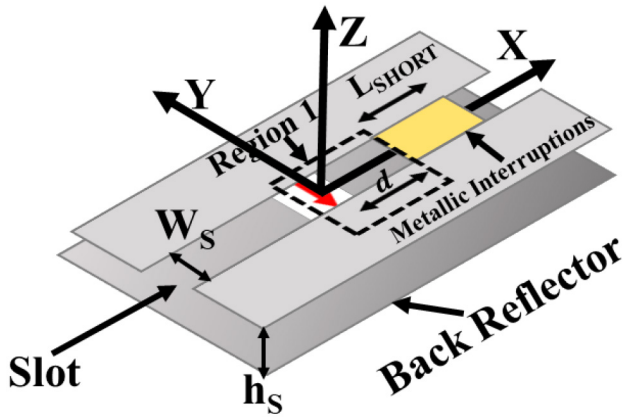
FIGURE 13. Semi-infinite slot in free space with the source. The semi-infinite slot is terminated by a short circuit of length L_{SHORT} placed at a distance d from the source. A BR is placed below the slot for directional radiation.
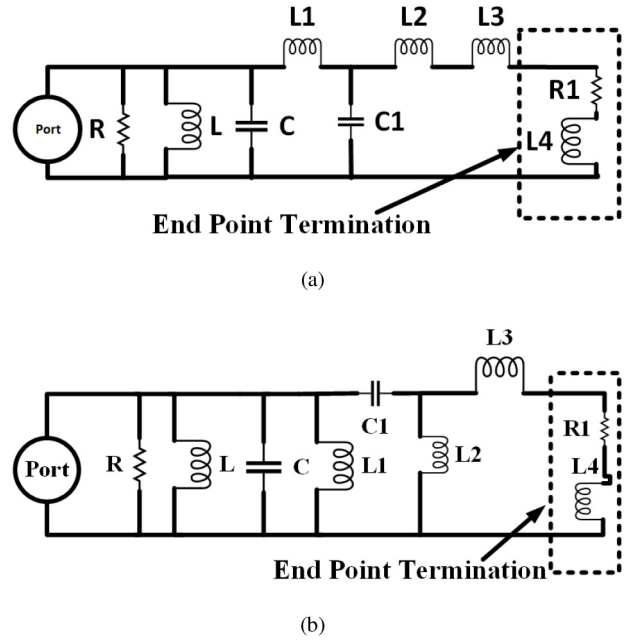

(a)

(b)

FIGURE 14. (a) RLC+T and (b) RLC+PI networks with RL load representing the endpoint of the semi-infinite slot (L_{SHORT}) in Fig. 13.

TABLE 2. Values of tuned and untuned L and C elements of the PI and T networks for semi-infinite slots. The unit of inductance is (nH) and the unit of capacitance is (fF).

Parameters	Values		Parameters	Values	
	Untuned	Tuned		Untuned	Tuned
L_{T1}	60	20.2	$L\pi_1$	60	250
C_{T1}	0.84	0.79	$C\pi_1$	0.21	0.55
L_{T2}	60	80.5	$L\pi_2$	60	26.5

used to compare the performance of the proposed equivalent circuit model. In the previous section, the infinite CSAA was presented where air was the separating medium between the CSAA and the BR. In this section, the semi-infinite CSAA is considered when it is printed on a dielectric substrate (i.e., $\epsilon_r > 1$). The input impedances of the semi-infinite slot for both the free space case and the case when the slot is printed on a dielectric substrate were calculated in [10]. It was shown that two resonances with narrower bandwidths are observed for the semi-infinite slot printed on a dielectric substrate. It is demonstrated in this section that the proposed equivalent circuit can capture and predict both resonances of the semi-infinite case when the slot is printed on a dielectric substrate.

Now, the proposed equivalent circuit is employed to find the input impedance of the semi-infinite slot. The circuit diagrams of the two topologies (i.e., PI and T networks), including the RL load termination, are depicted in Fig. 14. The RL loads in the figure are represented by R_1 and L_4. The operating frequency selected for this case is 1 GHz to show the applicability of the circuit model over various frequencies (in Section II, 28 GHz is demonstrated, and in this section, 1 GHz is selected). First, the values of different types of R, L, and C elements of the equivalent circuit are calculated using (7a)-(7c) and (10a)-(10d). The values of the RLC resonant circuit are $L = 37.5 nH$ and $C = 670 fF$. The tuned and untuned values of different L and C elements used for the PI and T networks are listed in Table 2.

The input impedance of the proposed equivalent circuit model of the semi-infinite slot antenna is calculated with the obtained circuit element values. The element values are tuned (as previously described), and the input impedance of the semi-infinite slot is plotted in Fig. 15. The input impedance is calculated in CST considering the following associated geometrical parameters, such as $d = 0.25\lambda_0$, $w_s = 0.02\lambda_0$, $\epsilon_r = 4$, $h = .05\lambda_d$ where h is the thickness of the dielectric substrate, λ_0 and λ_d are the wavelength in free space and with the dielectric substrate, respectively. The

impedance of the semi-infinite slot calculated by CST without (W/O) BR is taken from [10, Fig. 5]. The impedance of the semi-infinite slot along with the BR, which is placed at a quarter wavelength beneath the slot, is calculated in CST. The impedance of the RLC+PI and RLC+T networks is compared with the impedances obtained from CST (with and without BR) and from the MoM-based transmission line results presented in [10], [11], [12]. It is seen from Fig. 15 that the proposed equivalent circuit models capture both resonances at the lower and higher frequencies. The proposed circuit models capture the values of the impedance accurately at the lower resonance, while a noticeable deviation is observed at higher frequencies. On the other hand, there are discrepancies among the (RLC+PI and RLC+T) networks, the (CST W/O BR), and the MoM-based transmission line results. The disagreement is due to the fact that [10], [12] did not consider the presence of a back reflector within their CST and MoM-based solutions. However, the proposed equivalent RLC+T and RLC+PI networks are formulated considering the presence of a back reflector, which affects the behavior of the CSAA [2], [3], [13]. The percentage of error between the CST with BR results and the proposed lumped element-based RLC+PI and RLC+T equivalent circuit is calculated using (11). It is shown that excellent agreement
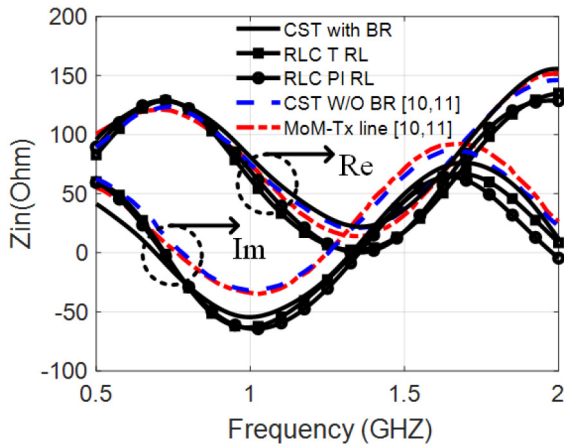
FIGURE 15. Comparison among the input impedances of the semi-infinite slot for different cases: CST (with and without BR), MoM based transmission line [10], [11], [12], and the proposed (RLC+T and RLC+T) networks.
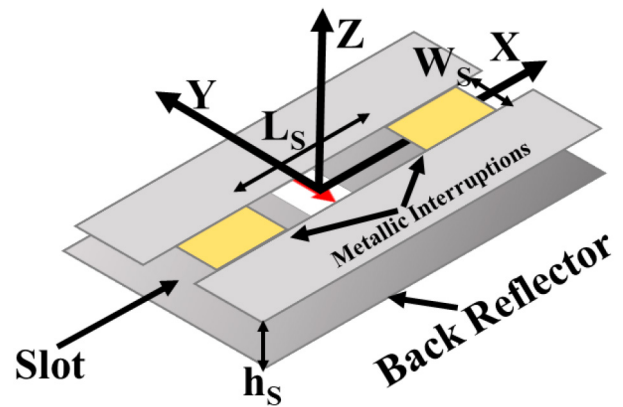

FIGURE 16. Planar finite slot in free space with the source. The slot is terminated at both ends. A BR is placed below the slot for directional radiation.
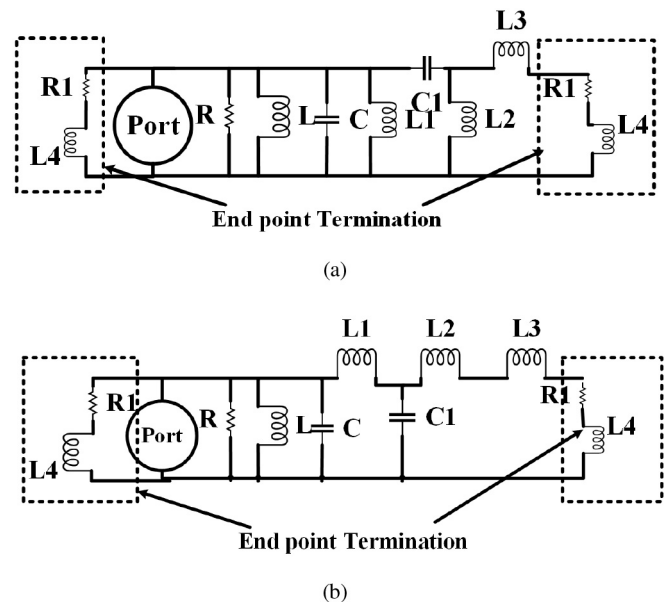

(a)

(b)

FIGURE 17. (a) RLC+PI and (b) RLC+T networks with two RL loads representing the two endpoints of the finite slot.

between the real impedances is observed at the lower resonant frequency and a maximum error of 5.8% is present for the higher resonant frequency. For the imaginary impedances, the maximum margin of error is 7.07% for the proposed equivalent circuits, which occur at 1.87 GHz. The average error for the real and imaginary parts of the impedances of the RLC+PI network is 2.53% and 3.11%, respectively. The average error for the real and imaginary parts of the impedances of the RLC+T network is 3.15% and 2.22%, respectively.

IV. FINITE SLOT

The semi-infinite planar slot discussed in the previous section is terminated on the remaining side to form the finite slot. A schematic of the planar finite slot in free space with BR is shown in Fig. 16. For the finite slots, there are two endpoint terminations. These two endpoint terminations are represented by two RL loads at the two sides of the slot, as discussed in the previous section. The equivalent circuit model of the planar finite slot includes the parallel RLC resonant circuit, the PI and T networks to denote the mutual coupling between the elements, the series inductor to represent the higher order modes, and the two RL loads for representing the two endpoints. The complete equivalent circuit diagram of the finite slot is shown in Fig. 17. It shows both the RLC+PI and RLC+T networks where the RL loads are represented by R_1 and L_4, respectively at the left and right corners of the circuit.

After designing the equivalent circuit for the finite slot, the impedances are calculated. The values of different elements are computed. To compare the results of the proposed equivalent circuit model, 1 GHz is chosen as the operating frequency. The values of the different R, L, and C are calculated using (7a)-(7c) and (10a)-(10d). The values of the RLC resonant circuit are found to be $L = 37.5nH$ and $C = 0.67pF$. Two cases are considered: one when the slot is in free space, and the other when the slot is printed on the dielectric substrate. Both equivalent circuit models based on PI and T networks are implemented and the impedance characteristics are calculated. The impedance of the finite slot in free space is calculated using CST considering the following relevant geometrical parameters, such as $L_s = 0.5\lambda_0$, and $w_s = 0.02\lambda_0$, where λ_0 is the wavelength in free space at f_0 [10], [12]. Subsequently, the impedance of the finite slot in free space is calculated in CST taking into consideration a BR placed quarter wavelength beneath the finite slot with similar antenna parameters.

The impedances (with and without BR) available from the CST and the MoM are compared with the impedances obtained from the lumped element-based equivalent circuits and are shown in Fig. 18. The impedance calculated by the MoM and CST without BR (W/O BR) is taken from [12]. It is understood from the figure that both networks (RLC+PI and RLC+T) can capture the resonance frequency and the
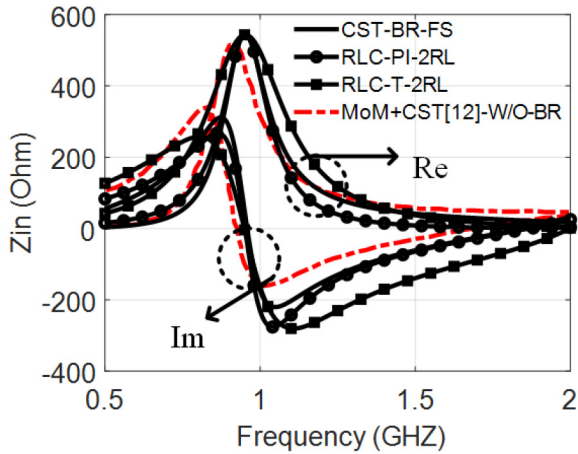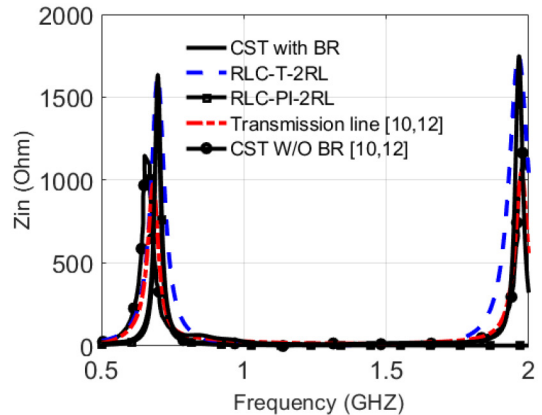
FIGURE 18. Comparison among the impedance of the finite slot in free space for different cases using CST (with and without BR), MoM-based transmission line [12], and the proposed RLC+T and RLC+T networks.

TABLE 3. Values of L and C elements of the PI and T networks for finite slots in free space (FS) and finite slot printed on a dielectric substrate (DS).

Parameters	Values	parameters	Values
L_{T1} (FS)	32.85 nH	$L\pi_1$ (FS)	51.07 nH
L_{T1} (DS)	24.75 nH	$L\pi_1$ (DS)	19.2 nH
C_{T1} (FS)	0.212c pF	$C\pi_1$ (FS)	0.53 pF
C_{T1} (DS)	0.58 pF	$C\pi_1$ (DS)	3.34 pF
L_{T2} (FS)	32.85 nH	$L\pi_2$ (FS)	14.5 nH
L_{T2} (DS)	24.75 nH	$L\pi_2$ (DS)	0.6 nH

(a)

(b)

FIGURE 19. Comparison among the (a) real part and (b) imaginary part of the impedance of the finite slot printed on a dielectric substrate for different cases using CST (with and without BR), MoM-based transmission line [12], and the proposed RLC+T and RLC+P networks.

value of the impedances. The RLC+PI network has better agreement with the CST-BR-FS results than the RLC+T network whereas the RLC+T network shows wider bandwidth. Disagreement between the results obtained through our equivalent circuit models (RLC+PI and RLC+T) and the CST+MoM results is observed. The disagreement of the results is due to the fact that [10], [12] did not consider the BR within their MoM-based solution for the finite slot. Moreover, these are the only available results in the literature against which the results of the proposed equivalent circuit model can be compared. The values of various L and C elements of the equivalent circuits are mentioned in Table 3. The tabulated values of the elements for the free space and dielectric substrate cases are different as they are a function of associated permittivity (ϵ) and permeability(μ).
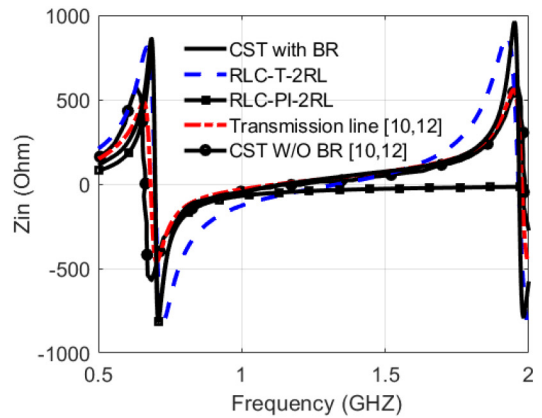
Now the considered case is the finite slot printed on a dielectric substrate. The selected operating frequency is 1 GHz. The impedance characteristics of the finite slot printed on the dielectric substrate are calculated using the obtained values from Table 3. The calculated results are compared with the MoM-based transmission line model and CST results [10], [12]. Various antenna parameters, such as $L_s = 0.5\lambda_0, w_s = 0.02\lambda_0, \epsilon_r = 4, h = .05\lambda_d$ are taken similar to [10], [12]. In addition, the impedance of the finite slot printed on the dielectric substrate with BR is calculated using CST. The comparisons among the real and imaginary parts of the impedances of the finite slot for different cases; CST (with and without BR), MoM-based transmission line [12], and the proposed RLC+T and RLC+P networks, are shown in Fig. 19(a) and 19(b), respectively. It is shown that the RLC+T network-based equivalent circuit is capable of capturing both resonance frequencies, and the values of the impedances match the (CST with BR) results. The RLC+PI network tracks only one resonant frequency with an impedance value equal to the (CST with BR) case, while it does not capture the second resonance at all. Disagreement exists among the results

of the (RLC+PI and RLC+T) networks, the CST (W/O BR), and the MoM-based transmission line. The reason is that [10], [12] did not consider the presence of BR within their MoM-based solution. Moreover, the conclusion drawn by the authors [10], [12] is that the transmission line captured the resonance of the higher frequency well but failed to capture the lower frequency resonance accurately. This drawback of the transmission line-based equivalent circuit is also demonstrated in Fig. 19. Thus, it is shown that the proposed

RLC+T network outperforms both the MoM-based transmission line model [10], [12] and the proposed RLC+PI network in capturing the resonance frequencies and impedance values.

The times needed to calculate the input impedance by the proposed equivalent circuit model and its full-wave counterpart are tabulated in Table 4. The simulations are performed on a computer with an Intel Core i7-7700 CPU @ 3.6GHz processor and 16 GB RAM. For both CST and the Quite Universal Circuit Simulator (QUCS) [19], 1001 sample points are considered. Different configurations of the CSAA (with and without BR) in free space and on a dielectric substrate are simulated in CST. The simulation times taken by CST are compared with the simulation time required by the proposed equivalent circuits in QUCS. For the infinite CSAA with BR configuration and the semi-infinite slot printed on a dielectric substrate (with and without BR), CST needs almost four hundred times more time than the proposed equivalent circuit models to give the impedance results. For the finite slot (with and without BR) in the free space case, CST is 175 times slower than the proposed equivalent circuit models. For the finite slot printed on a dielectric substrate case, CST is almost 400 times and 600 times slower than the proposed equivalent circuit models for without and with BR cases, respectively. Thus, the computation time advantage of the proposed circuit model is evident.

V. EFFECT OF VARIOUS SLOT PARAMETERS ON THE PROPOSED EQUIVALENT CIRCUIT MODEL

The effect of the various slot parameters (like the width of the slot, length of the slot, etc.) on the different circuit elements of the proposed equivalent circuit model is analyzed in this section. Please note that the values of the elements of the PI and T networks, series inductor (higher order mode representation), and RL loads (endpoint representation) are already set in previous Sections (II, III, and IV).

A. EFFECT OF SLOT WIDTH

The effect of the width of the slot, W_S on the proposed circuit model is investigated. W_S is varied from $0.05\lambda_0$ to $0.2\lambda_0$. The active impedance curves plotted in Fig. 20 show that the resonance of the CSAA shifts from a lower frequency to a higher frequency with the increase of the W_S. In addition, the bandwidth becomes wider as W_S is increased. W_S is related to the capacitance of the parallel resonant circuit of the proposed circuit model. Parametric sweeps are conducted on the value of C from the proposed circuit model for relating the effect. In Fig. 20, it is illustrated that the higher the value of C is, the lower the resonance of the proposed circuit model is. The phenomenon of obtaining wider bandwidth is also noticeable for lower values of C. Thus, it is understood that W_S is related to the value of C and there exists an inverse relationship between them.

B. EFFECT OF SLOT LENGTH

The effect of the length of the finite slot, L_S on the proposed circuit model is investigated. L_S is varied from 0.45λ to

TABLE 4. The simulation time for different cases.

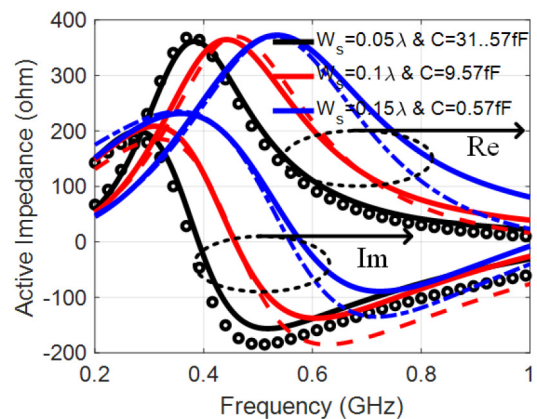| Case	CST without BR	CST with BR	Proposed equivalent circuit with BR	
			RLC+T network	RLC+PI network
Infinite slot in free space	——	28 s	69 ms	60 ms
Finite slot in free space	15 s	15 s	80 ms	89 ms
Semi-infinite slot printed on dielectric substrate	24 s	29 s	70 ms	70 ms
Finite slot printed on dielectric substrate	28 s	45 s	80 ms	70 ms

FIGURE 20. Active impedance of the CSAA for different widths of the slots W_S, calculated with CST and the proposed equivalent circuit model. The solid lines represent the impedances calculated by CST, while the dashed and dotted lines are calculated with the proposed equivalent circuit.

0.55λ. The active impedance curves plotted in Fig. 21 show that the resonance of the CSAA shifts from higher frequency values to lower ones with the increase of L_S. It is related to the inductance of the parallel resonant circuit of the proposed circuit model. Parametric sweeps are conducted on the value of L from the proposed circuit model to relate the effect. In Fig. 21, it is shown that the higher the value of L is, the lower the resonance of the proposed circuit model is. The resonance of the circuit model shifts to lower frequencies with the increase of L. Thus, it is seen that L_S is related to the value of L and there exists an inverse relationship between them.

C. PERIODICITY OF THE SLOTS

The periodicity (d_x, d_y) of the slots or the spacing between the elements in both x and y directions was included for calculating the active impedance of the CSAA in (1). While developing the proposed circuit model from (1), d_x and d_y are taken equal to 0.5λ. This consideration cancels both the d_y and d_x from the numerator and the denominator of (1).
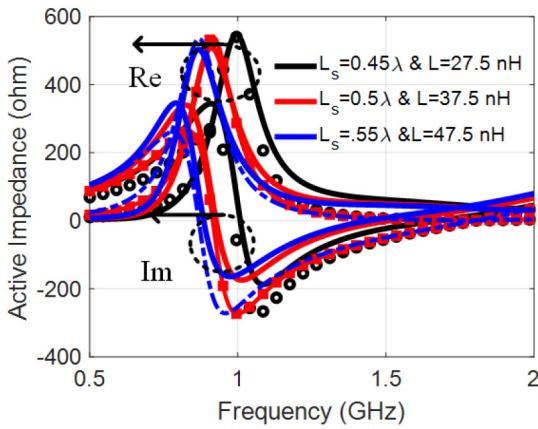
FIGURE 21. Active impedance of the CSAA for different lengths of the slots L_S calculated with CST and the proposed equivalent circuit model. The solid lines represent the impedances calculated by CST, while the dashed and dotted lines are calculated with the proposed equivalent circuit.

However, in the case when d_x and d_y are not equal, the active impedance of such scenarios can be obtained by a multiplicative factor based on the value of (d_y/d_x).

VI. PROTOTYPE VALIDATION

A 2x2 CSAA prototype was designed and fabricated to validate the results of the proposed lumped element-based equivalent circuit model of CSAA. The 2x2 CSAA prototype is printed on a RO3003 substrate with a dielectric constant $\epsilon_r = 3$ and a thickness of 1.52 mm. The BR is placed at a distance $\lambda_0/4$ below the ground plane [2]. The schematic view of the 2x2 CSAA prototype designed for 3 GHz operation is demonstrated in Fig. 22(a). The feeding network of the prototype is depicted in Fig. 22(b). It consists of three T-Junctions, tapered transmission lines, and radial stubs. The top view and bottom view of the fabricated prototype are shown in Fig. 22(c) and Fig. 22(d), respectively. The inter-element spacing in the x and y directions are $d_x = 0.41\lambda_0$ and $d_y = 0.54\lambda_0$, respectively. The various geometrical parameters of the 2x2 CSAA prototype are tabulated in Table 5.

The simulated and measured S parameters of the 2x2 CSAA prototype are plotted in Fig. 23, which show good agreement between them. The 2x2 CSAA prototype has 31% bandwidth and there is a slight shift between the measured and the simulated results, which can be attributed to the effects of the connector, cables, and other fabrication issues. The simulated far-field gain of the 2x2 CSAA prototype is 11.9 dBi having an efficiency of 94% and is shown in Fig. 24. The polar plot of the simulated and measured E-plane and H-plane is shown in Fig. 25. Very good agreement is demonstrated between the simulated and the measured radiation patterns. After this, the input impedance is calculated both from the simulated and measured S parameter results. The comparison between the simulated and measured input impedance is shown in Fig. 26. Slight discrepancy between the measured and the simulated input impedance
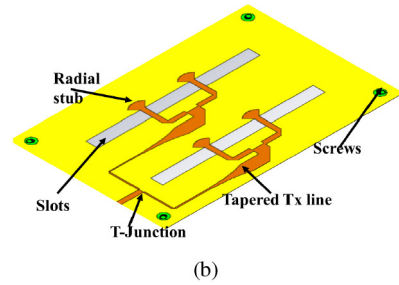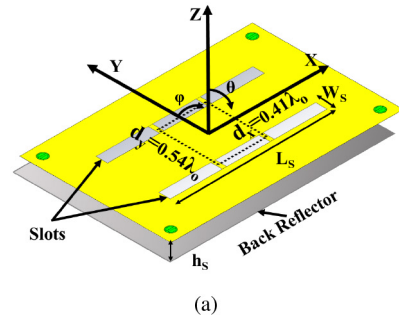

(a)

(b)

(c)

(d)

FIGURE 22. (a) Schematic view of the 2x2 CSAA prototype, (b) feeding network of the prototype, (c) fabricated top view of the 2x2 CSAA prototype, and (d) fabricated bottom view of the feeding network. The feeding network has three T-Junctions, tapered transmission lines, and radial stubs.

can be seen, which comes from the connector, cables, and other fabrication issues.

The equivalent circuit model of the 2x2 CSAA prototype is developed following Fig. 17. The proposed lumped element-based equivalent circuit model of the 2x2 CSAA prototype is shown in Fig. 27. The feed network of the prototype has three T-junctions, tapered lines, etc. The T-junctions are narrow band networks that can be represented with the help of an inductor and capacitor [16] as shown in Fig. 27(a). The complete lumped element-based equivalent circuit models (RLC+T and RLC+PI) including the feed network of the 2x2 CSAA prototype is depicted in Fig. 27(b) and Fig. 27(c), respectively. The value of the inductance and capacitance are tuned to obtain the input impedance. The input impedance obtained from this

TABLE 5. Geometrical parameters of 2x2 CSAA prototype.

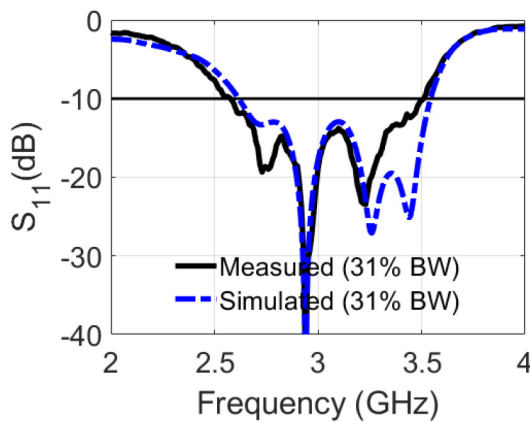| Parameter	Values (mm)	Parameter	Values (mm)
Length of the slot, L_s	135 ($1.35\lambda_0$)	Offset from edge	45 ($0.45\lambda_0$)
Width of the slot, W_s	10 ($0.1\lambda_0$)	Height of the back reflector	21 ($0.21\lambda_0$)
Spacing in x direction, d_x	41.07 ($0.41\lambda_0$)	Stub radius	10
Spacing in y direction, d_y	54 ($0.54\lambda_0$)	Feed length	22.85 ($0.22\lambda_0$)

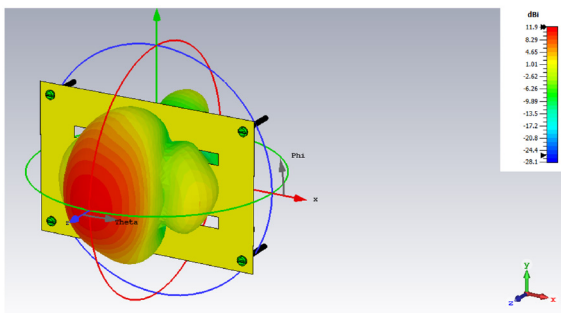FIGURE 23. Simulated (CST) and measured S parameters of 2x2 CSAA prototype.

FIGURE 24. Realized Gain of the 2x2 CSAA prototype.

(a)

(b)

FIGURE 25. Measured and simulated radiation pattern of the 2x2 CSAA prototype (a) E-plane ($\phi = 0^0$) and (b) H-plane ($\phi = 90^0$).

equivalent circuit model is compared with the measured and simulated (CST) results. The real and imaginary parts of the input impedance of the prototype are plotted in Fig. 26(a) and Fig. 26(b), respectively. The proposed circuit model of the prototype captures both the lower and upper resonance frequencies. The discrepancies between the measured and the proposed equivalent circuit model can be attributed to the effects of the cable, connector, homogeneity of the permittivity, and other fabrication-related issues, etc.

VII. DESIGN PROCEDURE
The design procedure of the proposed lumped element-based equivalent circuit (RLC+T and RLC+PI) is summarized here for all three configurations of the CSAA. This design procedure will assist in developing the equivalent circuit
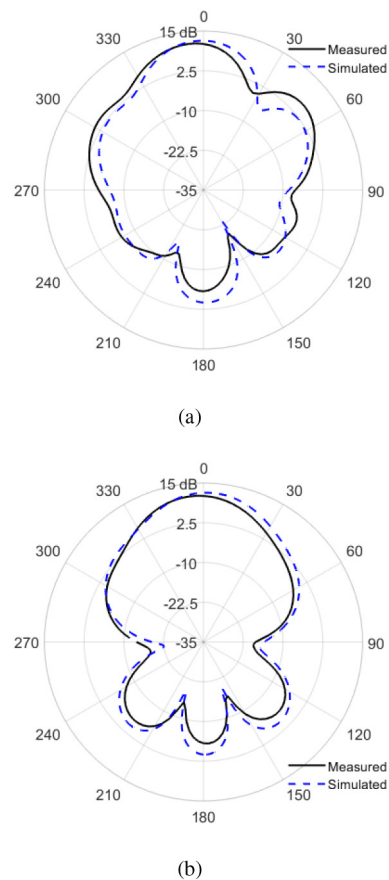
model of any configuration of CSAA at both microwave and mm-wave bands. The steps are as follows:

a) The center frequency f_c is to be selected first. It is assumed that there is a BR at a quarter wavelength distance beneath the CSAA to have a directional radiation pattern. Then, using (7a)-(7c), the values of the parallel resonant circuit elements such as R, L, and C, are to be calculated taking the values of f_c and h_s (height of the back reflector) into consideration. The resistance value, in this case, is equal to the free space intrinsic impedance as shown in [2].

b) The values of the elements of the PI and T networks are to be calculated using (10a)-(10d), after which, a series inductor is to be added to represent the higher-order modes present in the CSAA. Then, the input impedance and reflection characteristics of the infinite and periodic CSAA can be obtained in a circuit simulator like QUCS [19] (or any other SPICE-based simulator).

c) To determine the input impedance of the semi-infinite slot, the previous steps for infinite CSAA should be followed. In addition, the endpoint termination at one end of the slot is represented with an RL load. It is to be kept in mind that the values of the RL load vary depending on the width of the slots [12]. After obtaining all the values, the input impedance of the semi-infinite slot can be calculated in a circuit simulator.
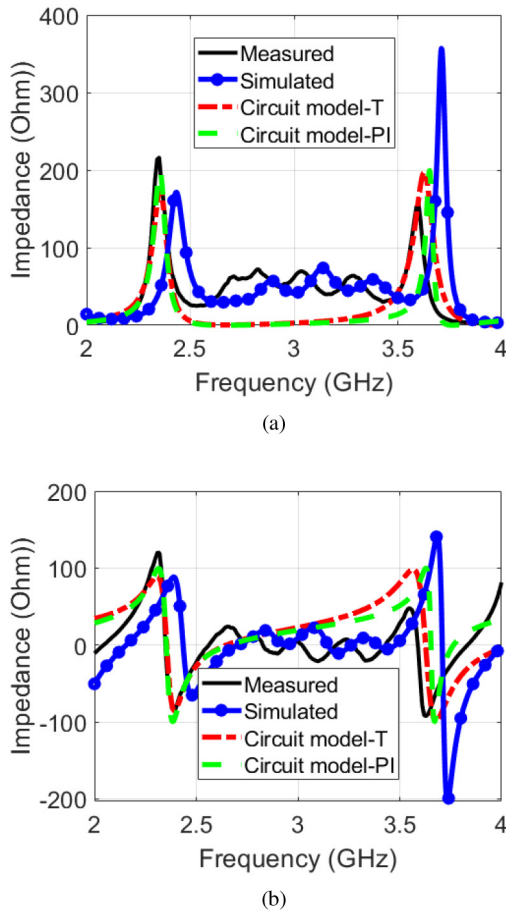
FIGURE 26. Comparison among the simulated (CST), measured, and proposed circuit model for the finite 2x2 CSAA prototype (a) real part of the input impedance, and (b) imaginary part of the input impedance.

FIGURE 27. (a) Equivalent circuit model of T-junctions [16], (b) proposed full lumped element circuit model (RLC+T), and (c) proposed full lumped element circuit model (RLC+PI).

d) The finite slot has two endpoint terminations, which can be represented by two RL loads. The values of the R, L, and C elements of the parallel RLC resonant circuit can be found as mentioned in step a). The procedures for finding the values of the PI and T network elements, and series inductor are discussed in step b). The RL values of the endpoints are discussed in step c). After obtaining all the element values, the input impedance and reflection characteristics of the finite slot can be obtained in a circuit simulator.

e) For the finite slot of real-time applications, the steps from a) to d) should be followed. Other components used in the CSAA should be modeled. For example, the feeding network, transmission lines, stubs, connectors, etc. should be included in the equivalent circuit model. The input impedance and reflection characteristics of the finite slot can then be obtained in the circuit simulator.

These steps will provide guidelines for developing the equivalent circuit for any configuration of the CSAA. As demonstrated in Table 4, the proposed equivalent circuit model will allow a quicker analysis of the input impedance and reflection characteristics of the CSAA. In addition, the
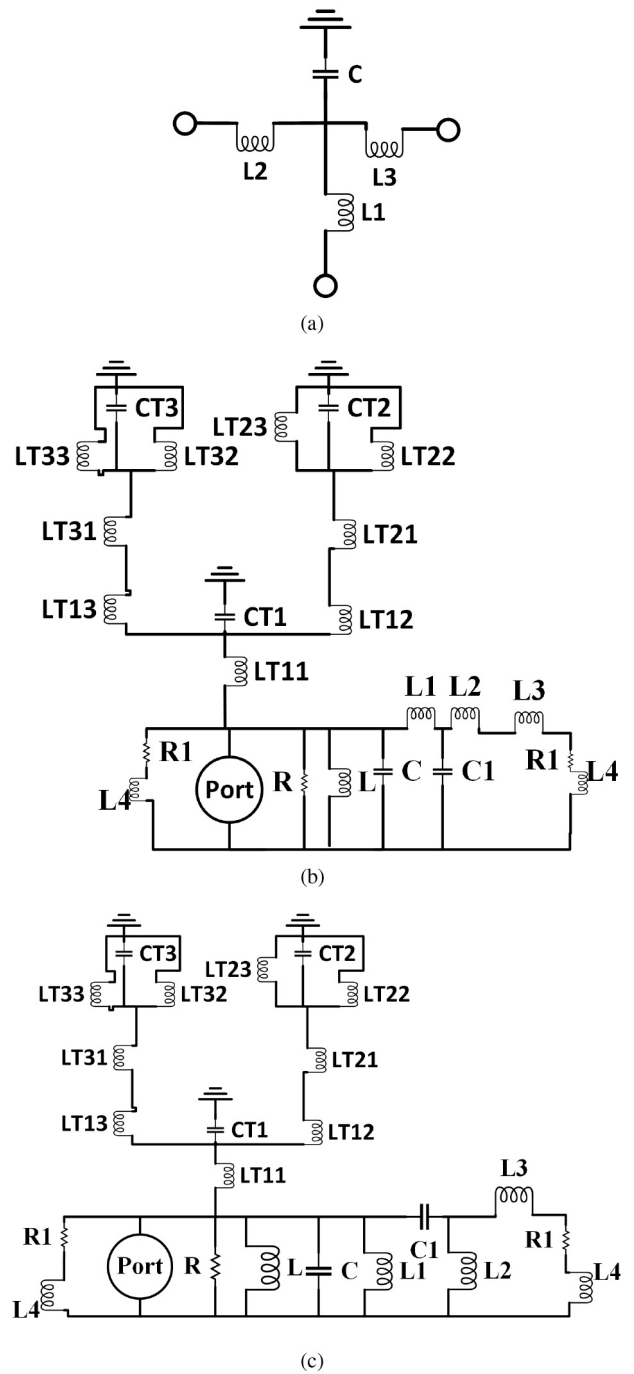
proposed equivalent circuit will help in modeling different geometrical parameters of CSAA before simulating the structure in a full-wave simulator.

The proposed model has a range of validity like any other meta-model. It is derived based on the analytical expressions from [2], [3], and [13]. Many approximations (like the width of the slot, the width of the source, etc.,) were considered to derive the input impedance curves. Therefore, the first limitation is that the proposed model is valid for narrow slots (i.e.,

$w_s = 0.1\lambda_0$ as shown in Section II-C) and excited by delta sources. This model is not applicable for designs with wider slots. Also, the proposed model is valid for the cases, where the radiation is directed towards the broadside. It may not be accurate in finding the impedance curves for slots where the beam is directed in another direction because the proposed design procedure and the equivalent circuit are based on equation (3). In addition, the model is used to design the CSAA at three different frequency bands. The infinite CSAA is designed at 28 GHz, the semi-infinite and finite slots are designed at 1 GHz, and the prototype is fabricated and tested at 3 GHz. Thus, this model will work with high accuracy at microwave and mm-wave bands. For higher frequency bands beyond 40 GHz (see Fig. 3), further investigations are required because second-order effects will become significant, which should not be neglected. Also, practical lumped element models should be considered. Finally, the proposed model is developed considering a square ($d_y = d_x$) periodic CSAA. However, the proposed model remains valid for the case of a rectangular slot, because it will change a constant multiplicative factor as shown in equation (1). This is discussed in Section V-C that a multiplicative factor is needed for rectangular planar CSAA to modify the input impedance following equation (1).

VIII. CONCLUSION

Complete lumped element-based equivalent circuit models for three different configurations of CSAA are presented. The viability and applicability of the proposed equivalent circuit comprising the RLC (fundamental mode), PI and T networks (coupling effects), and series inductor (higher order modes) have been demonstrated for infinite, semi-infinite, and finite CSAA. The impedance and reflection coefficient of the CSAAs are calculated and compared with the results of the GF and MoM-based (transmission line) equivalent circuits. The results are validated by CST and measured results. The proposed equivalent circuit of the infinite CSAA describes the resonance accurately and provides the full impedance and reflection behavior of the CSAA with 96% accuracy. The proposed circuit model for the semi-infinite CSAA describes the value of the impedance accurately at the lower resonance but shows errors (maximum of 5.8%) in describing the values of the impedance at higher frequencies. For the finite slot case, the proposed RLC+T network outperforms both the available transmission line-based equivalent circuit model from [10], [11], [12] and the proposed RLC+PI network in describing the resonance frequencies and the values of the impedances of the finite slot. The effects of various slot parameters, like width and the length of the slot, etc. on the proposed equivalent circuit model are investigated. To validate the proposed equivalent circuit model, a 2x2 CSAA prototype was built and measured. The comparison of the impedances between the proposed and measured results shows good agreement and accuracy. Three different operating frequencies (1 GHz, 3 GHz, and 28 GHz) were selected for designing various

configurations of the CSAA to demonstrate the scalability of the proposed equivalent circuit model. A generalized design procedure is presented for constructing and analyzing any CSAA configuration with the assistance of the proposed equivalent circuit model at both the microwave and mm-wave bands. The proposed equivalent circuit model will assist in the quicker analysis of the input impedance and reflection characteristics of the CSAA and help in modeling different antenna parameters before simulating the structure in a full-wave simulator. It is shown that the equivalent circuit model achieves 4.55% and 5.27% of maximum average error for real and imaginary impedances as compared with the full-wave simulator, while the computational time is reduced by more than two orders of magnitude.

REFERENCES

[1] R. C. Hansen, "Linear connected arrays," *IEEE Antennas Wireless Propag. Lett.*, vol. 3, no. 1, pp. 154–156, 2004.

[2] D. Cavallo, "Connected array antennas: Analysis and design," Ph.D. dissertation, Elect. Eng., Technische Universiteit Eindhoven, Eindhoven, The Netherlands, 2011.

[3] A. Neto, D. Cavallo, G. Gerini, and G. Toso, "Scanning performances of wideband connected arrays in the presence of a backing reflector," *IEEE Trans. Antennas Propag.*, vol. 57, no. 10, pp. 3092–3102, Oct. 2009.

[4] D. Cavallo, A. Neto, and G. Gerini, "Green's function based equivalent circuits for connected arrays in transmission and in reception," *IEEE Trans. Antennas Propag.*, vol. 59, no. 5, pp. 1535–1545, May 2011.

[5] D. Cavallo, W. H. Syed, and A. Neto, "Equivalent transmission line models for the analysis of edge effects in finite connected and tightly coupled arrays," *IEEE Trans. Antennas Propag.*, vol. 65, no. 4, pp. 1788–1795, Apr. 2017.

[6] Y. Wang and S. Chung, "A short open-end slot antenna with equivalent circuit analysis," *IEEE Trans. Antennas Propag.*, vol. 58, no. 5, pp. 1771–1775, May 2010.

[7] R. Garg, P. Bhartia, I. Bahl, and A. Ittipiboon, *Microstrip Antenna Design Handbook*. Norwood, MA, USA: Artech House, 2001.

[8] M. Himdi and J. P. Daniel, "Analysis of printed linear slot antenna using lossy transmission line model," *Electron. Lett.*, vol. 28, no. 6, pp. 598–601, 1992.

[9] J. E. Ruyle and J. T. Bernhard, "A wideband transmission line model for a slot antenna," *IEEE Trans. Antennas Propag.*, vol. 61, no. 3, pp. 1407–1410, Mar. 2013.

[10] R. M. van Schelven, D. Cavallo, and A. Neto, "Equivalent circuit models of finite slot antennas," *IEEE Trans. Antennas Propag.*, vol. 67, no. 7, pp. 4367–4376, Jul. 2019.

[11] R. van Schelven, D. Cavallo, and A. Neto, "Transmission line models of planar slot antennas," in *Proc. IEEE Antennas Propag. Soc. Int. Symp.*, Atlanta, GA, USA, 2019.

[12] R. van Schelven, D. Cavallo, and A. Neto, "Equivalent circuit models of finite slot antennas," in *Proc. 13th Eur. Conf. Antennas Propag. (EuCAP)*, Kraków, Poland, 2019.

[13] A. Neto and J. J. Lee, "Infinite Bandwidth" long slot array antenna," *IEEE Antennas Wireless Propag. Lett.*, vol. 4, pp. 75–78, 2005.

[14] D. Uznanski. "Series expansion. From mathWorld–A wolfram Web resource." Accessed: Feb. 11, 2021. [Online]. Available: https://mathworld.wolfram.com/SeriesExpansion.html

[15] A. McHutchon. "RLC resonant circuits." 2013. [Online]. Available: http://mlg.eng.cam.ac.uk/mchutchon/ResonantCircuits.pdf

[16] D. M. Pozar, *Microwave Engineering*, Hoboken, NJ, USA: Wiley, 2012.

[17] W. Richards, J. Zinecker, R. Clark, and S. Long, "Experimental and theoretical investigation of the inductance associated with a microstrip antenna feed," *Electromagnetics*, vol. 3, nos. 3–4, pp. 327–346, 1983.

[18] W. Richards, Y. Lo, and D. Harrison, "An improved theory for microstrip antennas and applications," *IEEE Trans. Antennas Propag.*, vol. 29, no. 1, pp. 38–46, Jan. 1981.

[19] "Quite universal circuit simulator." Accessed: Apr. 15, 2022. [Online]. Available: http://qucs.sourceforge.net

MD RASHEDUZZAMAN AL-AMIN (Graduate Student Member, IEEE) received the B.Sc. and M.Sc. degrees in electrical and electronic engineering from the Islamic University of Technology, Gazipur, Bangladesh, in 2011 and 2016, respectively. He is currently pursuing the Ph.D. degree with the Electrical Engineering Department, University of Montréal (Polytechnique Montréal), Montreal, QC, Canada. His research interests include microwave and millimeter-wave antenna design, phased array, connected antenna array, and antenna-in-package. He received the Fonds de Recherche du Québec Nature et Technologies (FRQNT) Doctoral Scholarship in 2020. He was a recipient of the 2021 IEEE Antennas and Propagation Society Doctoral Research Grant.

CHAO LI (Member, IEEE) received the B.S. degree in communication engineering from the North University of China in 2008, and the Ph.D. degree from Wuhan University in 2014. He is an Associate Professor with the School of Information Science and Engineering, Shandong Normal University, Jinan, China. In 2013, he was a visiting student with the Electromagnetic Communication Lab, Department of Electrical Engineering, Pennsylvania State University. From 2014 to 2015, he was a Postdoctoral Fellow with the University of Central Florida. From 2018 to 2021, he was with Polytechnique Montréal. His research interests include electromagnetic theory, computational electromagnetics, remote sensing, antenna, and microwave sensor.

MOHAMMAD S. SHARAWI (Senior Member, IEEE) is a Full Professor with the Electrical Engineering Department, University of Montréal (Polytechnique Montréal), Montreal, QC, Canada, where he is also a member of the Poly-Grames Research Center. He was with the King Fahd University of Petroleum and Minerals, Dhahran, Saudi Arabia, from 2009 to 2018, where he founded and directed the Antennas and Microwave Structure Design Laboratory. He was a Visiting Professor with the Intelligent Radio Laboratory, Department of Electrical Engineering, University of Calgary, Calgary, AB, Canada, in the Summer-Fall of 2014. He was a Visiting Research Professor with Oakland University, Rochester, MI, USA, in the Summer of 2013. He has more than 350 papers published in refereed journals and international conferences, 11 book chapters (two of which in the Antenna Handbook, 5th edition, McGraw Hill, 2018), one single authored book titled *Printed MIMO Antenna Engineering* (Artech House, 2014), and the Lead Author of the recent book *Design and Applications of Active Integrated Antennas* (Artech House, 2018). He has 25 issued/granted and 12 pending patents in the U.S. Patent Office. His research interests include multiband printed multiple-input-multiple-output (MIMO) antenna systems, reconfigurable and active integrated antennas, millimeter-wave MIMO antennas and integrated 4G/5G antennas, microwave sensors, applied electromagnetics, and computational methods. He was a recipient of the Abdul Hameed Shoman Foundation Award for Arab researchers for the category of wireless systems in 2020 in addition to the various best IEEE Conference Paper Awards. He is also serving as the Associate Editor for IEEE ANTENNAS AND WIRELESS PROPAGATION LETTERS, *IET Microwaves*, *Antennas and Propagation*, and IEEE OPEN JOURNAL ON ANTENNAS AND PROPAGATION and an Area Editor (Antennas and Microwave Devices and Systems) for *Microwave and Optical Technology Letters*. He is also the Specialty Chief Editor for the newly launched *Frontiers in Communications and Networks* for the System and Test-Bed Design Section. He has served on the technical and organizational program committees and organized several special sessions on MIMO antenna systems and architectures in several international conferences, such as EuCAP, IEEE Antennas and Propagation Society (APS), IMWS-5G, APCAP, and iWAT among many others for many years. He is also the APS Chair of the Montreal section and an Active Member of the IEEE Member Benefits Committee leading the initiative of the APS Student Travel Grant. He is also the Regional Delegate of the EuRAAP in North America.